JARO: 121–135 (2020)
DOI: 10.1007/s10162-020-00745-4

JARO
Journal of the Association for Research in Otolaryngology

Research Article

Myosin-XVa Controls Both Staircase Architecture and Diameter Gradation of Stereocilia Rows in the Auditory Hair Cell Bundles

Shadan Hadi,[1] Andrew J. Alexander,[1] A. Catalina Vélez-Ortega,[1] and Gregory I. Frolenkov[1]

[1]*Department of Physiology, College of Medicine, University of Kentucky, Lexington, KY 40536, USA*

Received: 29 August 2019; Accepted: 4 February 2020; Online publication: 9 March 2020

ABSTRACT

Mammalian hair cells develop their mechanosensory bundles through consecutive phases of stereocilia elongation, thickening, and retraction of supernumerary stereocilia. Many molecules involved in stereocilia elongation have been identified, including myosin-XVa. Significantly less is known about molecular mechanisms of stereocilia thickening and retraction. Here, we used scanning electron microscopy (SEM) to quantify postnatal changes in number and diameters of the auditory hair cell stereocilia in *shaker-2* mice (*Myo15*^{sh2}) that lack both "long" and "short" isoforms of myosin-XVa, and in mice lacking only the "long" myosin-XVa isoform (*Myo15*$^{\Delta N}$). Previously, we observed large mechanotransduction current in young postnatal inner (IHC) and outer (OHC) hair cells of both these strains. Stereocilia counts showed nearly identical developmental retraction of supernumerary stereocilia in control heterozygous, *Myo15*$^{sh2/sh2}$, and *Myo15*$^{\Delta N/\Delta N}$ mice, suggesting that this retraction is largely unaffected by myosin-XVa deficiency. However, myosin-XVa deficiency does affect stereocilia diameters. In control, the first (tallest) and second row stereocilia grow in diameter simultaneously. However, the third row stereocilia in IHCs grow only until postnatal day 1–2 and then become thinner. In OHCs, they also grow slower than taller stereocilia, forming a stereocilia diameter gradation within a hair bundle. The *sh2* mutation disrupts this gradation and makes all stereocilia nearly identical in thickness in both IHCs and OHCs, with only subtle residual diameter differences. All *Myo15*$^{sh2/sh2}$ stereocilia grow postnatally including the third row, which is not a part of normal development. Serial sections with focused ion beam (FIB)-SEM confirmed that diameter changes of *Myo15*$^{sh2/sh2}$ IHC and OHC stereocilia resulted from corresponding changes of their actin cores. In contrast to *Myo15*$^{sh2/sh2}$, *Myo15*$^{\Delta N/\Delta N}$ hair cells develop prominent stereocilia diameter gradation. Thus, besides building the staircase, the short isoform of myosin-XVa is essential for controlling the diameter of the third row stereocilia and formation of the stereocilia diameter gradation in a hair bundle.

Keywords: non-syndromic congenital deafness DFNB3, hearing, *shaker-2* mouse, development, mechanotransduction

INTRODUCTION

Mechanosensory bundles of the auditory hair cells consist of stereocilia that are arranged in rows of precisely defined heights, precise distances between the rows, and uniform stereocilia diameters within a row (Fig. 1a). It is generally believed that this characteristic shape of the stereocilia bundle is crucial for hair cell mechanosensitivity, albeit the exact relationship between architecture of the hair bundle and mechanotransduction is yet to be determined. Likewise, the exact mechanisms of how a cell could measure and develop such a precise hair bundle structure are largely unknown (Barr-Gillespie 2015).

Hair cell stereocilia arise from numerous microvilli-like projections through a series of consecutive

Correspondence to: Gregory I. Frolenkov · Department of Physiology, College of Medicine · University of Kentucky · Lexington, KY 40536, USA. email: Gregory.Frolenkov@uky.edu

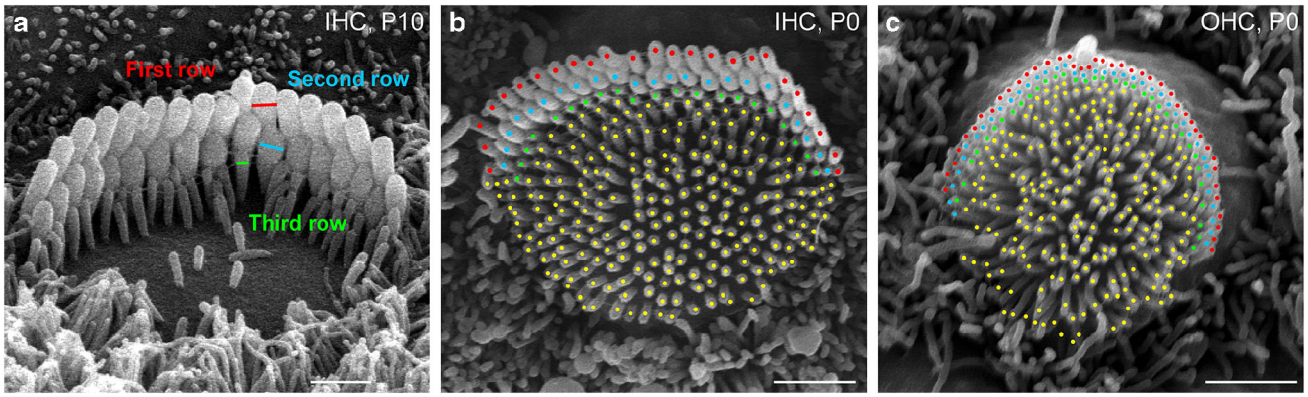

FIG. 1. Hair bundle development and quantification of stereocilia number and diameters. **a** SEM image of a relatively mature inner hair cell (IHC) bundle at the middle of the cochlea in a control mouse at postnatal day 10 (P10). Note the well-organized three rows of stereocilia that form a staircase. Examples of diameter measurements are illustrated by lines of different colors in the first (red), second (cyan), and third (green) rows of stereocilia. **b**, **c** "Top view" of the control IHC (**b**) and an OHC (**c**) immature stereocilia bundles at P0 in the same mid-cochlear location with all nascent stereocilia (stereocilia-like projections) marked. Identifiable stereocilia rows are indicated with markers of different colors. Scale bars 1 μm

developmental stages that are generally similar in chick and rodents, even though the shape of stereocilia bundles in these species is quite different (Tilney and Tilney 1986; Kaltenbach et al. 1994). The most studied stage is the differential elongation of stereocilia, which results in the characteristic "staircase" architecture of the hair bundle. Unconventional myosin-XVa is the first molecule that was identified as crucial for stereocilia elongation (Probst et al. 1998; Wang et al. 1998). It is localized to the tips of stereocilia (Belyantseva et al. 2003; Rzadzinska et al. 2004), the site of stereocilia growth where new monomers are added to the barbed ends of unidirectionally aligned actin filaments (Tilney et al. 1980; Schneider et al. 2002). Myosin-XVa interacts with the scaffold protein whirlin (Belyantseva et al. 2005; Delprat et al. 2005) and transports it to the tips of stereocilia (Belyantseva et al. 2005). The actin-regulatory protein EPS8 and the complex of G protein signaling modulator 2 (GPSM2) and inhibitory G proteins alpha (GNAI) both interact with myosin-XVa/whirlin and are also transported to the tips of stereocilia (Manor et al. 2011; Zampini et al. 2011; Tadenev et al. 2019). When this macromolecular complex arrives to the stereocilia tips, it initiates stereocilia elongation (Belyantseva et al. 2005; Manor et al. 2011). Another potential component of this complex, EPS8L2, may not contribute to stereocilia elongation in development but seems to be responsible for maintaining the proper stereocilia heights in mature hair bundles (Furness et al. 2013). Besides the myosin-XVa-dependent macromolecular complex, the heights of stereocilia can be regulated by proteins with actin-capping activity such as twinfilin-2 (Peng et al. 2009) and the actin-binding proteins ESPN-1 and ESPNL. The latter proteins interact with different isoforms of myosin-III, also forming macromolecular complexes at the tips of stereocilia (Schneider et al. 2006; Salles et al. 2009; Merritt et al. 2012; Ebrahim et al. 2016; Lelli et al. 2016).

In contrast to stereocilia elongation, the mechanisms of other stages of hair bundle formation are almost unexplored. An essential step in shaping the hair bundle is the retraction of supernumerary microvilli (Tilney et al. 1992; Kaltenbach et al. 1994) (compare also Fig. 1a and b). However, to the best of our knowledge, the mechanisms of this retraction have never been investigated. Likewise, programmed elongation of stereocilia is accompanied by their progressive widening (Tilney and Tilney 1986; Kaltenbach et al. 1994), which must include assembly of additional actin filaments in the stereocilium core and recruitment of specific actin-bundling proteins that are essential for stereocilia widening, such as espin, plastin-1, and fascin (Sekerkova et al. 2011; Krey et al. 2016). However, the mechanisms linking stereocilia elongation and their widening are also unknown.

Here, we show that the myosin-XVa-based complex is essential not only for stereocilia elongation but also for determining precise gradation of stereocilia diameters between stereocilia rows within a hair bundle. This study was inspired by observations that whirlin deficiency results in increase of stereocilia diameters (Mogensen et al. 2007) as well as our own qualitative observations on the diameters of stereocilia in inner and outer hair cells (IHCs and OHCs) of *shaker-2* mice (Stepanyan and Frolenkov 2009), which lack functional myosin-XVa in their stereocilia (Belyantseva et al. 2003). We systematically measured the diameters of stereocilia in different rows of IHC and OHC bundles on scanning electron microscopy (SEM) images at

different ages during development from postnatal day 0 (P0) until postnatal day 21 (P21). We compared IHC and OHC stereocilia of control normal-hearing heterozygous (*Myo15*$^{+/sh2}$) and mutant homozygous *shaker-2* (*Myo15*$^{sh2/sh2}$) mice. Since hair cells express two different isoforms of myosin-XVa, with or without a long N-terminus extension (Belyantseva et al. 2003; Fang et al. 2015), we also quantified IHC and OHC stereocilia diameters in mice lacking only the "long" isoform of myosin-XVa (*Myo15*$^{\Delta N/\Delta N}$) (Fang et al. 2015). Our measurements demonstrate that only the absence of both myosin-XVa isoforms eliminates the differences in diameters between stereocilia rows in IHC and OHC bundles. Using focused ion beam electron microcopy (FIB-SEM), we obtained serial sections of control and *Myo15*$^{sh2/sh2}$ stereocilia in IHCs and OHCs and reconstructed their longitudinal views. We confirmed that nearly identical diameters of *Myo15*$^{sh2/sh2}$ stereocilia within a hair bundle are supported by equally thick actin cores. We concluded that the "short" but not "long" isoform of myosin-XVa is a key molecule that is essential not only for elongation of stereocilia but also for gradation of their diameters within a hair bundle. Preliminary reports on this study were presented at ARO meetings (2017–2019).

METHODS

Mice

We used *shaker-2* (*Myo15*^{sh2}, stock no. 000109, Jackson Lab) mice that have a p.C592Y point mutation inactivating motor domain of myosin-XVa (Belyantseva et al. 2003; Belyantseva et al. 2005) and the isoform-specific knockout mice that lack the long splice isoform of myosin-XVa (Fang et al. 2015). The latter mice were generated with a p.E1086X mutation in *Myo15* exon 2, equivalent to p.E1105X in humans. We refer to this allele as *Myo15*$^{\Delta N}$ for convenience, and we genotyped these mice by taking advantage of an *MseI* site introduced by the mutation (Fang et al. 2015). For genotyping, tail snip samples were extracted from mouse pups and genomic DNA was purified using the Wizard® SV Genomic DNA Purification System (Promega, Madison, WI) and eluted in 500 µl. PCR was performed using Taq DNA polymerase (Promega). Primers and PCR conditions were described previously (Belyantseva et al. 2005; Fang et al. 2015).

Usually, we bred heterozygous/homozygous pairs that generate *Myo15*$^{+/sh2}$ and *Myo15*$^{+/\Delta N}$ controls as well as *Myo15*$^{sh2/sh2}$ and *Myo15*$^{\Delta N/\Delta N}$ mutants. Previous studies demonstrated normal hearing in heterozygous *Myo15*$^{+/sh2}$ and *Myo15*$^{+/\Delta N}$ mice (Karolyi et al. 2003; Fang et al. 2015). Several mice of each genotype were euthanized for subsequent organ of Corti dissection and preparation for electron microscopy at different postnatal ages, from P0 until P21. The day of birth was designated as P0. By P21, all developmental changes in both IHC and OHC bundles are largely completed (Kaltenbach et al. 1994).

All animal procedures were approved by the University of Kentucky Animal Care and Use Committee (protocol no. 903M2005).

Tissue Preparation for SEM

Mouse temporal bones were carefully dissected in cold Leibovitz (L-15) solution to extract the cochleae. Neonatal cochleae (ages less than P5) were micro-dissected, and organs of Corti were fixed in 1 mL of 3 % formaldehyde plus 3 % of glutaraldehyde in 0.1 M sodium cacodylate buffer (pH = 7.4), supplemented with 2 mM of $CaCl_2$ that was added to fixative prior to use. The tectorial membrane was removed prior to fixation using fine forceps. Older cochleae (> P5) were gently perfused with the above fixative through the oval window using a fine needle and then post-fixed overnight at 4 °C. This step was essential to prevent damage of the hair cells in the basal region of the organ of Corti. After 24 h, approximately 6 mL of distilled water was added to dilute the fixative and prevent over-fixation of the tissue. The organs of Corti were micro-dissected in the following days. All samples were dehydrated with graded series of ethanol as follows: 5 %,10 %, 20 %,40 %, 60 %, 80 %, and 100 % with at least 20-min incubation at room temperature after each step and an overnight incubation in 100 % ethanol after the final step. The samples were then critical point dried with liquid CO_2 using Leica EM CPD300 automated critical point dryer. Dried samples were carefully mounted on 14 mm Hitachi aluminum holders using double-stick carbon tape (EMS catalog no. 77825-12) and sputter coated with 5 nm of platinum (Q150T equipped with film thickness monitor; Quorum Technologies, Guelph, Canada) for subsequent SEM imaging.

SEM Imaging

We used field-emission scanning electron microscopes (S-3400 Hitachi or Helios Nanolab 660, FEI, Hillsboro, OR) to image IHC and OHC bundles approximately in the middle of the cochlea. We imaged at least six neighboring IHCs and OHCs in each sample from control heterozygous and mutant homozygous mice. To keep a reasonable compromise between a relatively large field of view and a decent resolution, magnification was set to include three hair cells in one image. Proper measurements of stereocil-

ia heights require an estimate of the angle of sample surface relative to the electron beam (Velez-Ortega et al. 2017). Two images of the same bundles, a front and a top view, were sufficient for this estimation and subsequent data analysis.

Serial Sectioning with FIB-SEM

After euthanasia, temporal bones from control and *Myo15*$^{sh2/sh2}$ mice (P8), one animal per genotype, were carefully dissected in cold Leibovitz (L-15) media. Cochleae were perfused through the oval window with 3 % formaldehyde plus 3 % of glutaraldehyde in 0.1 M sodium cacodylate buffer (pH = 7.4), supplemented with 2 mM of $CaCl_2$ and 1 % tannic acid (EMS catalog no. 21710). Perfused cochleae were stored in 1 mL of fixative for overnight incubation at room temperature. In the following day, organs of Corti were micro-dissected and cut into pieces to obtain the preferable region in the middle of the cochlea. They were stored for 24 h at 4 °C in distilled water without removal of tectorial membrane. Samples were cryoprotected with increasing concentrations of glycerol (EMS cat no. 16550): 5 %, 10 %, 15 %, 20 %, and 25 % for at least 20 min and final overnight incubation in 30 % glycerol at room temperature. Next, organ of Corti samples were frozen in liquid nitrogen using the Leica EM ICE high-pressure freezer and transferred to 1 % uranyl acetate in methanol at − 90 °C in a Leica EM AFS2 freeze substitution machine. Methanol was exchanged for Lowicryl HM-20 resin and polymerized by UV light. All reagents were obtained from Electron Microscopy Sciences. The resin blocks were trimmed on an ultramicrotome (UC6, Leica, Wetzlar, Germany) to reach a desired sample distance of 20–50 µm from the upper surface of the block. The samples were serial sectioned with a focused ion beam at a 20-nm step size and imaged in "Slice and View" mode with a backscattered electron detector using the FEI Helios 660 Nanolab system.

Data Analysis: Stereocilia Number and Diameters

Using ImageJ software (ver.1.51), we manually counted the total number of stereocilia per bundle in IHCs and OHCs. Usually, it was easy to recognize the borders of a hair cell in the "top view" SEM images, even in the immature hair cells at P0 (Fig. 1b, c). IHC stereocilia were well-organized into a bundle at P0, making their count a relatively simple task (Fig. 1b). OHC stereocilia seem to be less stiff at this age and, therefore, they appeared sometime similar to the microvilli of the neighboring supporting cells (Fig. 1c). In these cases, we used two or three independent observers to count the number of stereocilia—more precisely, stereocilia-like projections—in the same cell. We have found that independent counts differ by no more than ten stereocilia. This is about 3 % of the total number of stereocilia in the OHCs at P0 and significantly less than the cell-to-cell variability (Fig. 3d). To measure stereocilia diameters, a straight line was drawn perpendicular to the axis of a stereocilium (at the thickest region in case of a second row stereocilium in the IHCs) and the length between the edges was recorded (Fig. 1a). In developing IHCs, stereocilia diameters are relatively uniform only in the middle of the hair bundle. Therefore, we excluded from the analysis at least three stereocilia at the edges of each stereocilia row. Even though OHC stereocilia are more uniform within a row, we have used the same strategy of selecting stereocilia in the middle of a bundle for OHCs too. We averaged stereocilia diameters for each cell first and then used the number of cells rather than the number of stereocilia for statistical analysis.

The data were plotted and analyzed with the OriginPro 2020 software, which could handle missing data in ANOVA analysis. Statistical significance was determined either by *t* test of independent variables with Welch correction or by two-way ANOVA with Bonferroni ad hoc test. See figure legends for specific details. Figures were assembled using Adobe Illustrator CC (2017.1.0 Release).

The width of the actin core of stereocilia in *shaker-2* IHCs and OHCs was measured in control heterozygous *Myo15*$^{+/sh2}$ and mutant *Myo15* $^{sh2/sh2}$ mice at P8. We chose this age because this is approximately the middle of developmental maturation of the IHC bundle and our SEM data showed prominent gradation of stereocilia diameters at this age. We analyzed a stack of serial FIB-SEM sections with Fiji software (ImageJ2 ver.1.52n). Location of a stereocilium within specific row was confirmed with Fiji's 5-D orthogonal viewer. The widths of actin cores of the first, second, and third row stereocilia were measured at the stereocilium's thickest region as in Fig. 1a, with a line drawn perpendicular to actin filaments.

Data Analysis: Stereocilia Heights

First, serial FIB-SEM sections were registered and aligned using a custom-written MATLAB script. Then, the stack was calibrated for correct voxel size (typically 1.5–2 nm in X and Y, and 20 nm in Z). Longitudinal sections through the stereocilia were reconstructed from these aligned FIB-SEM stacks. A straight line was drawn through each stereocilium to generate a dynamic "re-slice view" of that specific stereocilium. Position of this line was adjusted by following the stereocilium in several consecutive slices to confirm that the resliced view reveals the entire stereocilium

from the tip to the rootlet. Then, the height of a stereocilium was determined as a distance from the cuticular plate surface to the stereocilium tip.

3D Reconstruction of FIB-SEM Stack

After FIB-SEM stack registration and calibration, we generated a "sub-stack" by selecting consecutive slices that collectively reveal stereocilia within the different rows of the hair bundle. Images within this sub-stack were inverted and median filtered. Maximum intensity projections were generated by "Z-project" function of Fiji software.

RESULTS

Myosin-XVa Is Not Essential for Developmental Retraction of the Supernumerary Stereocilia in the Auditory Hair Cells

Since nothing is known about the molecules regulating the developmental retraction of supernumerary stereocilia in the hair cell bundles, we first explored whether myosin-XVa is involved in this process. Therefore, we tracked the changes of the total number of stereocilia per hair bundle throughout postnatal development (P0-P21). Our data show that starting from birth (P0), all control heterozygous and mutant homozygous *Myo15*^{sh2} and *Myo15*$^{\Delta N}$ IHC bundles have a large number of stereocilia, ~200–300 per bundle. Later, this number decreases more than twofold through the retraction of the supernumerary microvilli-like stereocilia over the course of 6 days (P0-P6) (Fig. 2a, d). After P6, the total number of stereocilia decreases very slowly throughout the adult age in both control *Myo15*$^{+/sh2}$ and *Myo15*$^{sh2/sh2}$ IHCs (Fig. 2d, left). Although two-way ANOVA analysis did not reveal the overall statistical significance between the number of stereocilia in *Myo15*$^{+/sh2}$ and *Myo15*$^{sh2/sh2}$ IHCs, fit to the logistic function showed that the total number of stereocilia plateaued at a slightly higher value in *Myo15*$^{sh2/sh2}$ IHCs (*Myo15*$^{+/sh2}$: 67.8 ± 14.6 stereocilia/cell; *Myo15*$^{sh2/sh2}$: 89.1 ± 2.6 stereocilia/cell). This difference was due to delayed retraction of the residual stereocilia-like projections at the cuticular plate surface in *Myo15*$^{sh2/sh2}$ IHCs (Fig. 2a, b, arrows). In contrast to *Myo15*$^{sh2/sh2}$ IHCs, number of stereocilia per bundle continues to decrease in *Myo15*$^{\Delta N/\Delta N}$ IHCs after P6 (Fig. 2d, right) due to selective degeneration of the second and third row in the adult bundles, which confirms previous observations (Fang et al. 2015). This degeneration results in overall statistical significance between the number of stereocilia in *Myo15*$^{+/\Delta N}$ and *Myo15*$^{\Delta N/\Delta N}$ IHCs (two-way ANOVA, $P < 0.001$). Thus, despite subtle differences from control, the overall programmed retraction of supernumerary stereocilia is not affected in either *Myo15*$^{sh2/sh2}$ or *Myo15*$^{\Delta N/\Delta N}$ mice. Therefore, we conclude that neither the long nor the short isoform of myosin-XVa is essential for the resorption of supernumerary stereocilia in the IHC bundles during postnatal development.

Similarly, quantification of the total number of stereocilia per OHC bundle shows a largely identical retraction of supernumerary stereocilia in control, *Myo15*$^{sh2/sh2}$, and *Myo15*$^{\Delta N/\Delta N}$ OHCs (Fig. 3). This reduction in stereocilia number seems to be steeper in the OHCs than in IHCs since OHCs have initially a larger number of nascent stereocilia (compare Figs. 2d and 3d). Similar to IHCs, logistic fit revealed that *Myo15*$^{sh2/sh2}$ OHCs maintain a slightly larger number of stereocilia in the adult postnatal ages (P16–20) compared to that in the control (*Myo15*$^{+/sh2}$: 74.2 ± 29.9 stereocilia/cell; *Myo15*$^{sh2/sh2}$: 98.9 ± 4.8 stereocilia/cell), also due to delayed retraction of stereocilia-like projections (Fig. 3b, arrow). Overall, neither short nor long isoform of myosin-XVa disrupts the programmed retraction of the supernumerary stereocilia in the OHC bundles. Therefore, we conclude that myosin-XVa is not essential for the programmed retraction of supernumerary microvilli within the auditory hair bundles.

Myosin-XVa Is Essential for Stereocilia Diameter Gradation Between the Rows of the IHC Bundle

Since myosin-XVa is essential for the elongation of stereocilia (Probst et al. 1998), we were curious whether it is also needed to determine the mature thickness of stereocilia. Therefore, we measured the diameters of stereocilia in all three rows in control, *Myo15*$^{sh2/sh2}$, and *Myo15*$^{\Delta N/\Delta N}$ IHC bundles at P0-P21 (Fig. 4). These measurements show that in order to achieve the proper wild-type-like architecture, stereocilia of the first (tallest) and second row of control IHCs continuously increase in thickness, reaching a maximum diameter of approximately 325–340 nm by P16. Both first and second row stereocilia show no significant difference in their diameter growth throughout postnatal development (Fig. 4d, f, left). In contrast to the taller rows, diameters of the third row stereocilia behave differently. There is an initial increase in stereocilia thickness during the first postnatal days P0-P1, which then remains steady up to P4–6, followed by a small continuous reduction in stereocilia diameters (Fig. 4d, f, left). This developmental arrest of the growth with subsequent thinning in the row 3 stereocilia is a major contributor to the diameter gradation within the rows of the IHC bundle (Fig. 4a).

In contrast to normal IHCs, gradation of stereocilia diameters in *Myo15*$^{sh2/sh2}$ IHC bundles was

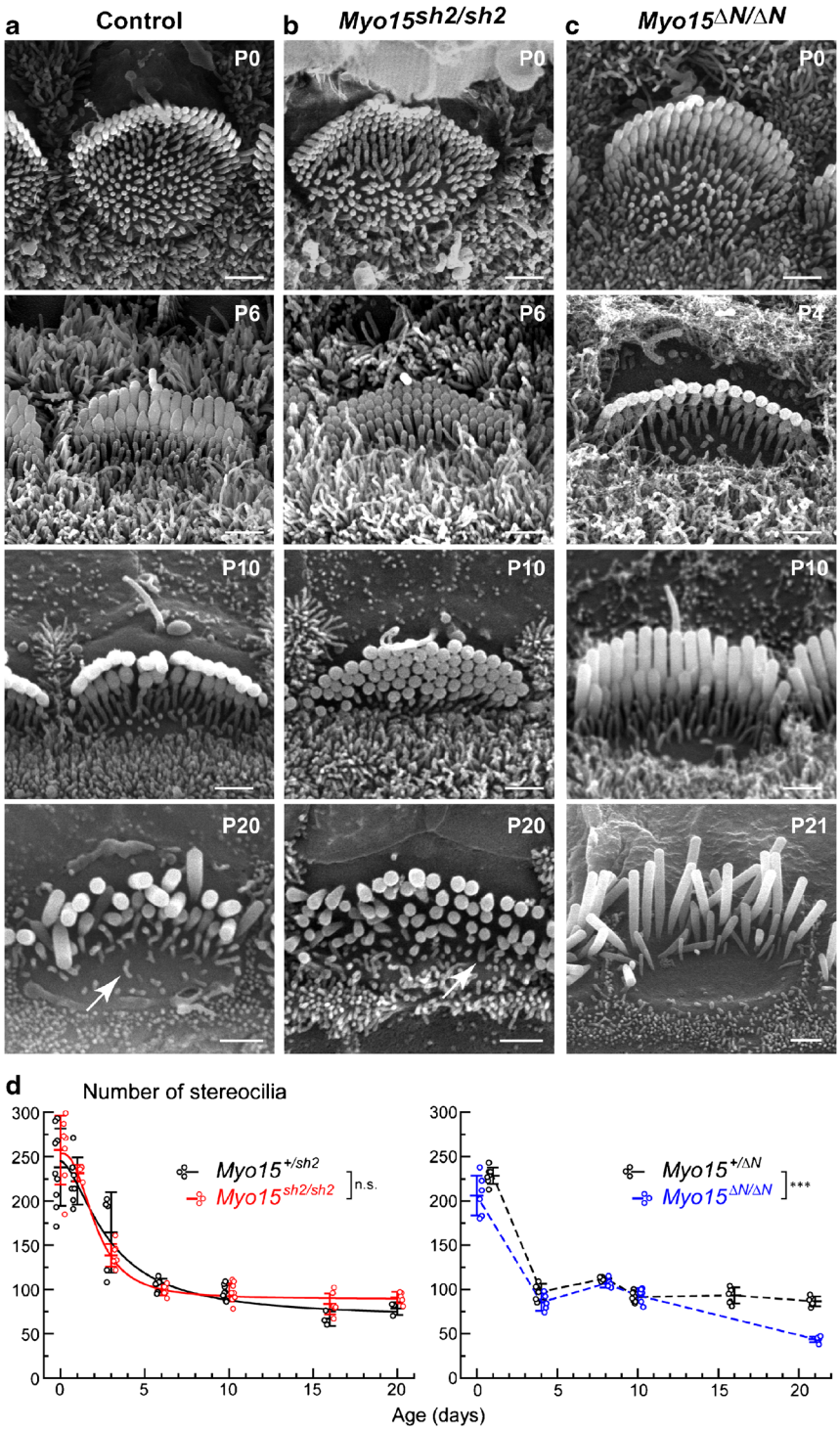

FIG. 2. Myosin-XVa is not essential for developmental retraction of supernumerary stereocilia in IHCs. **a–c** SEM images of control heterozygous (*Myo15*$^{+/sh2}$) (**a**), mutant *Myo15*$^{sh2/sh2}$ (**b**), and mutant *Myo15*$^{\Delta N/\Delta N}$ (**c**) IHC bundles at different postnatal ages, P0-P21. Scale bars: 1 µm. Arrows point to the examples of stereocilia-like projections remaining at the cuticular plate surface of control and *Myo15*$^{sh2/sh2}$ IHCs at P20. **d** Total number of first, second, and third row stereocilia plus stereocilia-like projections in the IHC bundles of *Myo15*$^{sh2/sh2}$ (red, left), *Myo15*$^{\Delta N/\Delta N}$ (blue, right), and control heterozygous mice of the same strains (black). Each data point represents individual IHC and is artificially plotted with a small offset relative to the vertical whiskers with a central mark that shows mean ± standard deviations (SDs). All cells were located in the middle of the cochlea. Each time point combines the data from two to three independent biological samples (mice) of each genotype. Asterisks indicate statistical significance of the differences of stereocilia numbers between the rows (two-way ANOVA: n.s., non-significant; $^{*}P<0.05$; $^{**}P<0.01$; $^{***}P<0.001$). Data for *Myo15*^{sh2} strain were fitted to the logistic function, $y = A_2 + (A_1\text{-}A_2)/(1 + (x/x_0)\text{^}p)$, with the following parameters (±SD): *Myo15*$^{+/sh2}$ IHCs, $A_1 = 245 \pm 43$, $A_2 = 67.8 \pm 14.6$, $x_0 = 2.87 \pm 1.33$ days, $p = 1.65 \pm 0.98$; *Myo15*$^{sh2/sh2}$ IHCs, $A_1 = 254 \pm 13$, $A_2 = 89.1 \pm 2.6$, $x_0 = 2.12 \pm 0.26$ days, $p = 2.52 \pm 0.43$. Unfortunately, we did not have enough data for a reliable fit to the logistic function for *Myo15*$^{\Delta N}$ strain

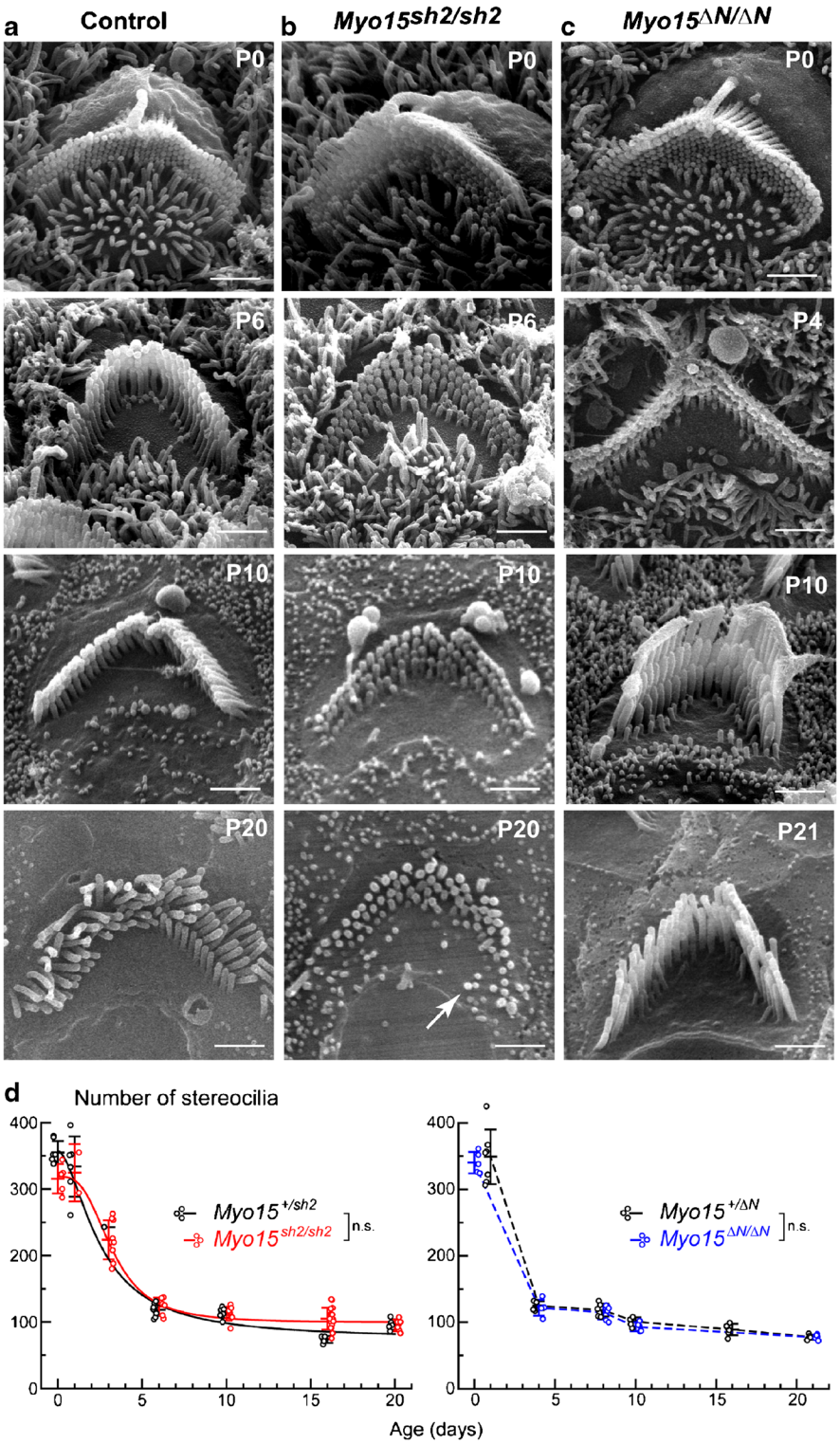

FIG. 3. Myosin-XVa is not essential for developmental retraction of supernumerary stereocilia in OHCs. **a**–**c** SEM images of control heterozygous (*Myo15*$^{+/sh2}$) (**a**), mutant *Myo15*$^{sh2/sh2}$ (**b**), and mutant *Myo15*$^{\Delta N/\Delta N}$ (**c**) OHC bundles at different postnatal ages, P0-P21. Scale bars: 1 µm. Arrow points to an example of stereocilia-like projection remaining at the cuticular plate surface of *Myo15*$^{sh2/sh2}$ OHCs at P20. **d** Total number of first, second, and third row stereocilia plus stereocilia-like projections in the OHC bundles of *Myo15*$^{sh2/sh2}$ (red, left), *Myo15*$^{\Delta N/\Delta N}$ (blue, right), and control heterozygous mice of the same strains (black). All cells were located in the middle of the cochlea. Each time point combines the data from two to four independent biological samples (mice) of each genotype, except $n = 1$ for control *Myo15*$^{+/sh2}$ OHCs at P3. All other details of the layout are as in Fig. 2. Coefficients of the fits to the logistic function in panel **d** (left): *Myo15*$^{+/sh2}$ OHCs, $A_1 = 356 \pm 45$, $A_2 = 74.2 \pm 29.9$, $x_0 = 2.5 \pm 1.9$ days, $p = 1.7 \pm 1.7$; *Myo15*$^{sh2/sh2}$ OHCs, $A_1 = 318 \pm 12$, $A_2 = 98.9 \pm 4.8$, $x_0 = 3.23 \pm 0.32$ days, $p = 3.07 \pm 0.68$

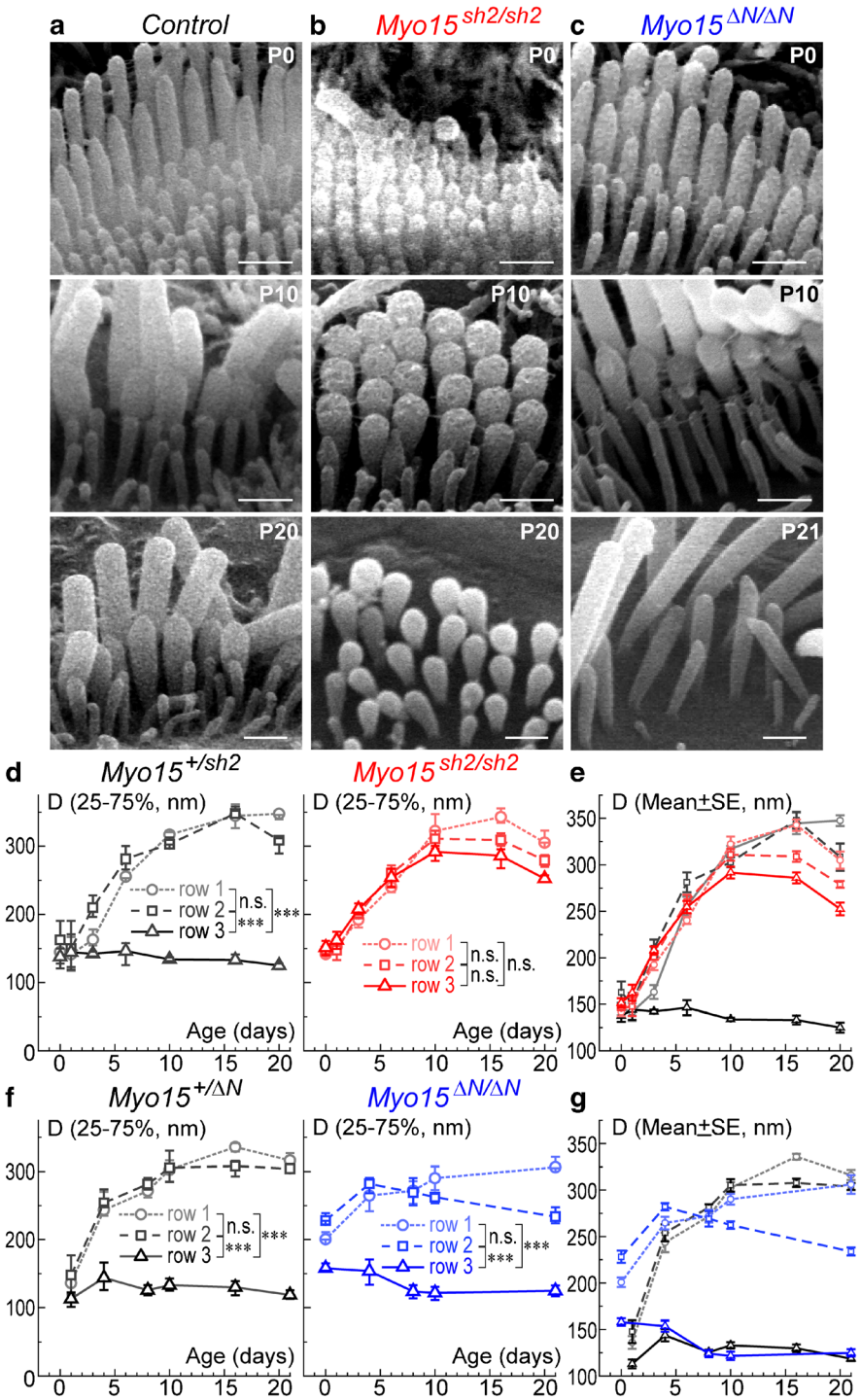

FIG. 4. Gradation of stereocilia diameters is lost in *Myo15*$^{sh2/sh2}$ but not *Myo15*$^{\Delta N/\Delta N}$ IHCs. **a**–**c** Magnified SEM images of IHC stereocilia in control (**a**), *Myo15*$^{sh2/sh2}$ (**b**), and *Myo15*$^{\Delta N/\Delta N}$ (**c**) mice at different postnatal ages. Scale bars: 0.5 µm. **d**–**g** Quantification of stereocilia diameters (*D*, nm) in the first (circles, dotted lines), second (squares, dashed lines), and third (triangles, solid lines) stereocilia rows of the *Myo15*$^{sh2/sh2}$ (different shades of red) and *Myo15*$^{\Delta N/\Delta N}$ (different shades of blue) IHC bundles, as well as in corresponding heterozygous controls (different shades of gray/black). Panels **d**–**f** show mean values with 25–75 % confidence intervals, while panels **e**–**g** re-plot the data on an expanded Y-scale as mean ± standard error of mean (SE) to highlight differences between stereocilia rows and/or genotypes. Asterisks indicate statistical significance of the differences of stereocilia diameters between the rows (two-way ANOVA with Bonferroni correction: n.s., non-significant; $*P<0.05$; $**P<0.01$; $***P<0.001$). To separate confounding issues of stereocilia degeneration in mutants, statistical analysis was performed with P0-P16 data, since both *Myo15*$^{sh2/sh2}$ and *Myo15*$^{\Delta N/\Delta N}$ IHCs show some signs of stereocilia diameter degradation at P20–21 (see panels **e**–**g**). All cells were from the middle of the cochlea, and all measured stereocilia were located in the middle of the bundle (excluding at least three stereocilia at the edges of each stereocilia row). Number of cells: 4–16 from at least two different mice per age/genotype

hardly noticeable (Fig. 4b) and, overall, the differences in the diameters of stereocilia in different rows of *Myo15*$^{sh2/sh2}$ IHC bundle were statistically non-significant at P0-P16 (Fig. 4d, right). Analysis of developmental changes revealed that this happens because the third row stereocilia continue to grow through postnatal development in *Myo15*$^{sh2/sh2}$ IHCs (Fig. 4d, right). Overall, third row stereocilia in *Myo15*$^{sh2/sh2}$ IHC bundles are significantly thicker than that in control IHC bundles (Fig. 4e). This abnormality of the third row stereocilia was not observed in *Myo15*$^{\Delta N/\Delta N}$ IHC bundles (Fig. 4c), implicating that the short but not the long isoform of myosin-XVa controls the diameter of the third row stereocilia in IHCs. In *Myo15*$^{\Delta N/\Delta N}$ IHC, first and second row stereocilia grow in diameter similarly (or even faster) than that in control at P0-P4 (Fig. 4f, right; Fig. 4g). From P8-P10 onward, the second row stereocilia in *Myo15*$^{\Delta N/\Delta N}$ IHCs became thinner (Fig. 4f, right). This result is consistent with a previous report that demonstrated thinning of the second row stereocilia in the *Myo15*$^{\Delta N/\Delta N}$ IHCs that begins at P8 (Fang et al. 2015). The third row stereocilia have significantly smaller diameters than the stereocilia of the first and second rows throughout all studied ages (Fig. 4f, right), indicating that the normal developmental inhibition of the stereocilia diameter growth in the third row is maintained in *Myo15*$^{\Delta N/\Delta N}$ IHCs.

Although there is a prominent disruption in the normal diameter gradation in *Myo15*$^{sh2/sh2}$ stereocilia bundles, we did observe some residual gradation that becomes significant during a late postnatal period (P16-P20). Yet, this gradation was very different. In control bundles, first and second rows had similar stereocilia diameters, while the third row stereocilia were significantly thinner (Fig. 4d, f, left). In contrast, in *Myo15*$^{sh2/sh2}$ IHCs, we observed small but gradual differences in stereocilia diameters from the first to the third row (Fig. 4d, right).

Myosin-XVa Regulates the Differences in Stereocilia Diameters in the OHC Bundles

We imaged and measured the diameters of stereocilia in all three rows of OHC bundles in control, *Myo15*$^{sh2/sh2}$, and *Myo15*$^{\Delta N/\Delta N}$ mice at P0-P21 (Fig. 5). In control OHC bundles, stereocilia diameters in all rows increase throughout postnatal development. Thickness gradation becomes noticeable from ~P4 and continues through late in development (Fig. 5d, f left). First and second row stereocilia were not significantly different in thickness, unlike third row stereocilia which were significantly thinner than the taller rows (Fig. 5d, f, left). As we expected, the gradation of stereocilia diameters in different rows largely disappeared during development (P0-P10) in *Myo15*$^{sh2/sh2}$ OHCs that lack both long and short isoforms of myosin-XVa (Fig. 5d, right). At these ages, third row stereocilia were thicker in *Myo15*$^{sh2/sh2}$ OHCs than in control OHCs, and as thick as the first and second row in *Myo15*$^{sh2/sh2}$ OHCs (Fig. 5e). Similar to IHCs, we did observe a very subtle gradient of stereocilia diameters from first to third row stereocilia in *Myo15*$^{sh2/sh2}$ OHCs (Fig. 5e). After P10, there was a decline in thickness of stereocilia in all rows of *Myo15*$^{sh2/sh2}$ OHC bundle that may indicate their degeneration (Fig. 5e). Like in IHCs, stereocilia diameter gradation was not affected in *Myo15*$^{\Delta N/\Delta N}$ OHC bundles that lack only long isoform of myosin-XVa (Fig. 5c, f, right). In these bundles, first and second row stereocilia develop similarly to the control (albeit, a bit faster), and third row stereocilia are significantly thinner starting from P0, forming an evident gradation of diameters within the bundle. Thus, we conclude that the short isoform of myosin-XVa, but not the long one, maintains thickness gradation within the rows in OHCs.

Actin Core in Myosin-XVa-Deficient Stereocilia

To explore the changes of the actin core associated with myosin-XVa deficiency, we obtained at least one 3D stack of 20-nm FIB-SEM serial sections in control *Myo15*$^{+/sh2}$ and mutant *Myo15*$^{sh2/sh2}$ IHCs (Fig. 6a, b) and OHCs at P8, in the middle of the developmental maturation of IHC bundles. Although this FIB-SEM dataset has a limited number of cells, it is useful for comparison of stereocilia dimensions within the same hair bundle. As expected, we observed the loss of gradation of stereocilia core diameters in *Myo15*$^{sh2/sh2}$ IHC (Fig. 6c) and OHC (Fig. 6d) bundles. In full correspondence to our previous observations (Stepanyan and Frolenkov 2009), measurements of stereocilia core heights in *Myo15*$^{sh2/sh2}$ hair cells revealed no detectable staircase architecture in *Myo15*$^{sh2/sh2}$ IHC bundles (Fig. 6e) and diminished but still present staircase in *Myo15*$^{sh2/sh2}$ OHC bundles (Fig. 6f). Interestingly, all stereocilia within *Myo15*$^{sh2/sh2}$ IHC bundle have well-developed rootlets, including stereocilia of the fourth and fifth rows (Fig. 6b). However, the rootlets of these stereocilia often had a “wiggled” appearance. In the control IHCs, these supernumerary stereocilia are normally in the retracting phase at this age. It is yet to be determined whether and how the rootlets may contribute to the stereocilia retraction program in postnatal development.

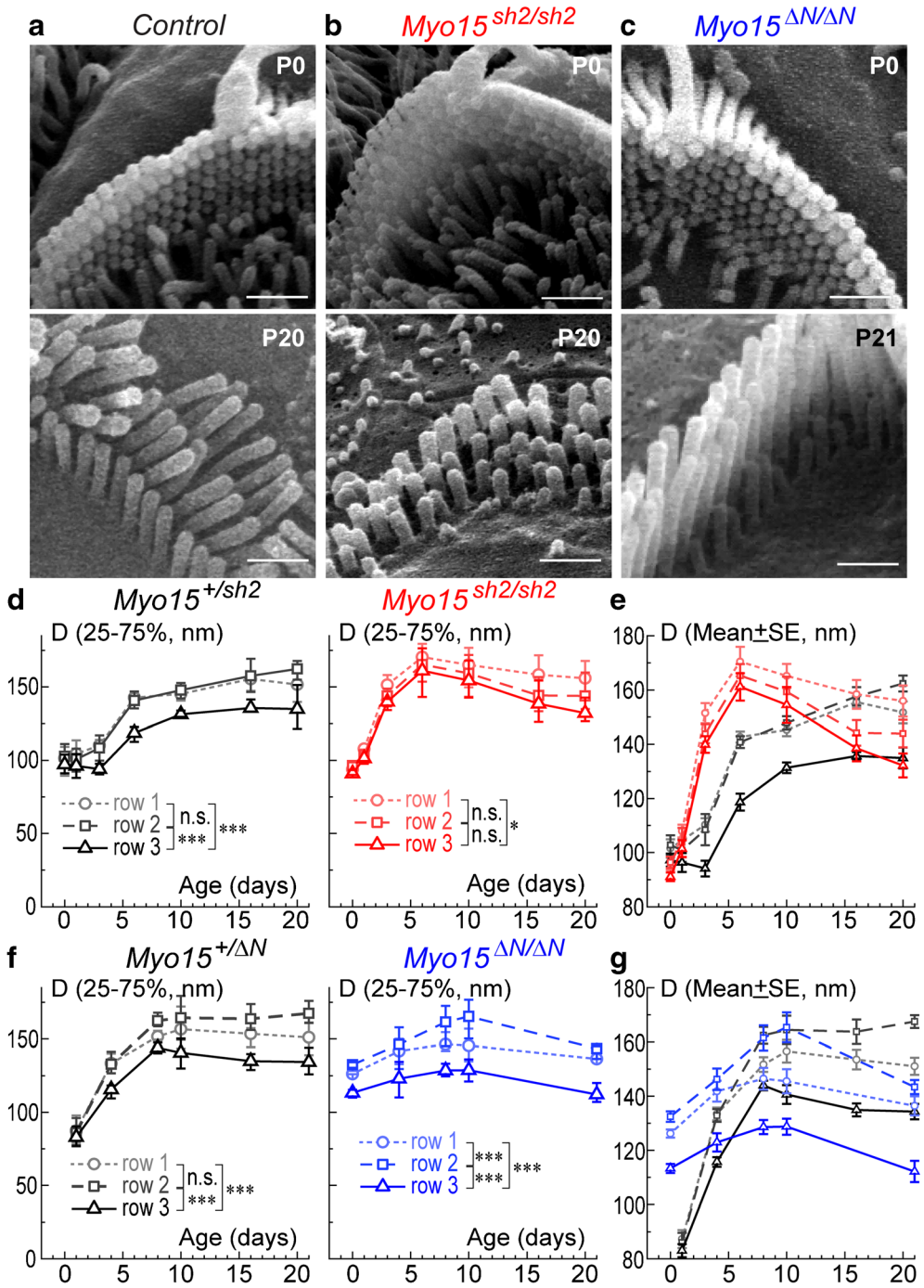

FIG. 5. Gradation of stereocilia diameters is lost in *Myo15*$^{sh2/sh2}$ but not *Myo15*$^{\Delta N/\Delta N}$ OHCs. **a**–**c** Magnified SEM images of stereocilia in control (**a**), *Myo15*$^{sh2/sh2}$ (**b**), and *Myo15*$^{\Delta N/\Delta N}$ (**c**) OHCs at different postnatal ages. Scale bars: 0.5 µm. **d**–**g** Quantification of stereocilia diameters (*D*, nm) in the first (circles, dotted lines), second (squares, dashed lines), and third (triangles, solid lines) stereocilia rows of the *Myo15*$^{sh2/sh2}$ (different shades of red) and *Myo15*$^{\Delta N/\Delta N}$ (different shades of blue) OHC bundles, as well as in corresponding heterozygous controls (different shades of gray/black). Other details of the layout are as in Fig. 4. Statistical analysis was performed with P0-P10 data, since both *Myo15*$^{sh2/sh2}$ and *Myo15*$^{\Delta N/\Delta N}$ OHCs show some signs of stereocilia diameter degradation at P16–21 (see panels **e**–**g**). All cells were from the middle of the cochlea, and stereocilia at the very edges of the rows were excluded from analysis. Number of cells: 4–15 from at least two different mice per age/genotype

DISCUSSION

This study establishes that the myosin-XVa-based stereocilia elongation complex affects gradation of stereocilia diameters within hair bundles of the auditory hair cells. Effects of myosin-XVa deficiency on stereocilia diameters were long suspected based on qualitative examination of SEM images of IHC

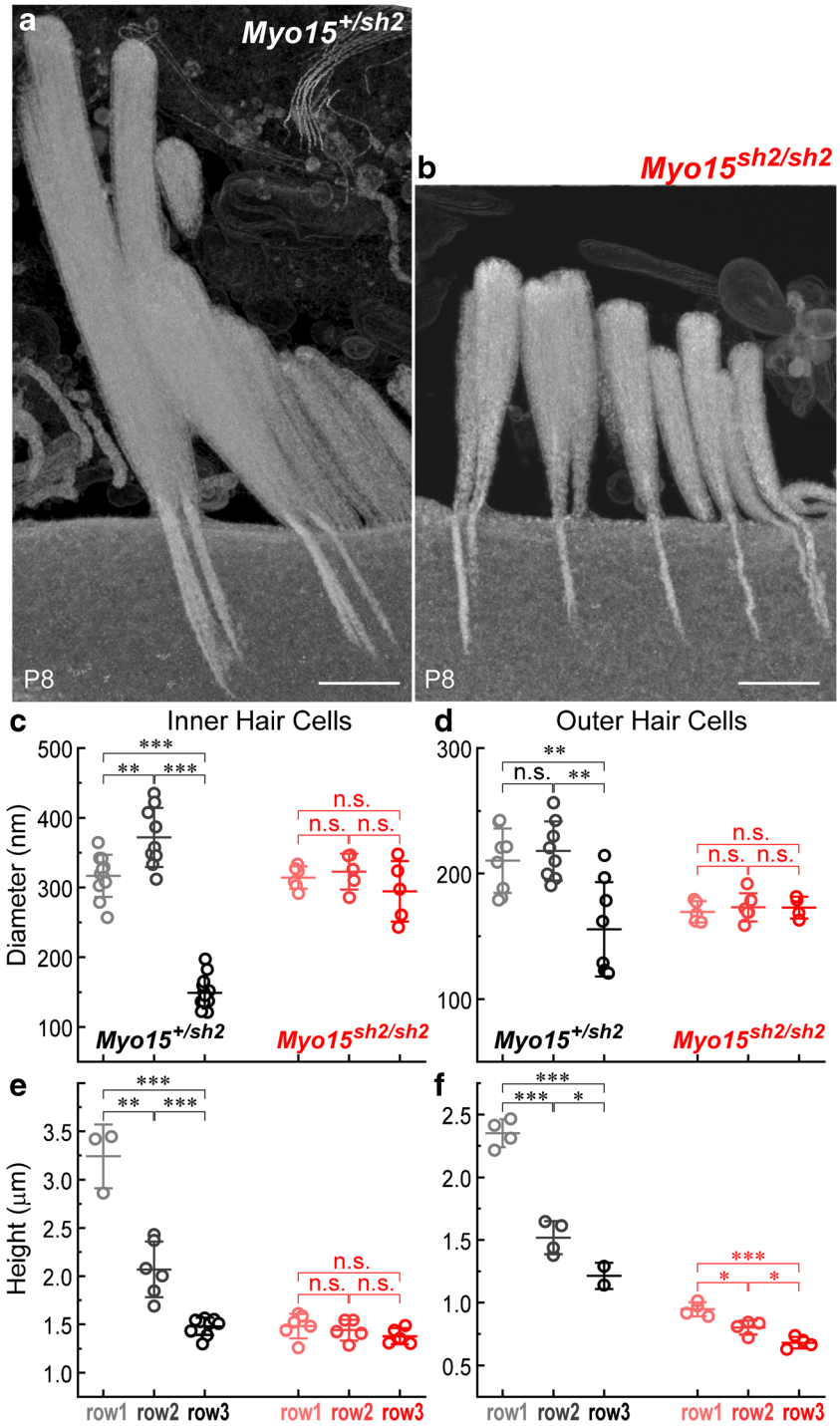

FIG. 6. Reorganization of stereocilia actin core in *Myo15*$^{sh2/sh2}$ mice. **a**, **b** Reconstruction of the longitudinal views of stereocilia bundles in the IHCs of *Myo15*$^{+/sh2}$ (**a**) and *Myo15*$^{sh2/sh2}$ (**b**) mice from 20-nm-thick FIB-SEM serial sections. Scale bars: 500 nm. **c**–**f** Quantification of stereocilia diameters (**c**, **d**) and heights (**e**, **f**) from 3D FIB-SEM stacks of images of IHC (**c**–**e**) and OHC (**d**–**f**) bundles. Each data point represents one stereocilium in the first, second, or third stereocilia rows of the bundle (shown in different shades of gray for *Myo15*$^{+/sh2}$ stereocilia or different shades of red for *Myo15*$^{sh2/sh2}$ stereocilia). All measured stereocilia were located in the middle of the bundle (excluding at least three stereocilia at the edges of each stereocilia row). Mean values ± SD are also shown. Asterisks indicate significance of the differences (*t* test of independent variables: n.s., non-significant; $^{*}P<0.05$; $^{**}P<0.01$; $^{***}P<0.001$). All cells were located in the middle of the cochlea of P8 mice. Because sample preparation and serial sectioning with FIB-SEM is still a labor- and time-consuming procedure, serial sections of only one bundle per hair cell type/genotype were obtained (except two control IHCs)

bundles but have never been systematically investigated. Our measurements demonstrated that the gradation of stereocilia diameters between the rows in a hair bundle is formed by the selective inhibition of the developmental growth of the third row stereocilia in both IHCs and OHCs. The short isoform of myosin-XVa seems to be an essential molecule for this process.

Myosin-XVa Is Not Essential for Programmed Resorption of Supernumerary Stereocilia

The retraction of supernumerary stereocilia in development is accompanied by widespread reduction in the number and the heights of microvilli in all neighboring supporting cells (see SEM images on Fig. 2a–c and Fig. 3a–c). Therefore, auditory hair cells may have a conserved mechanism that favors systemic elimination of the supernumerary stereocilia and protects true stereocilia. The mechanisms that determine the fates of stereocilia and microvilli are linked to the differences in their actin dynamics (Gorelik et al. 2003; Drummond et al. 2015; Narayanan et al. 2015). In contrast to the initial findings postulating that F-actin in mammalian hair cell stereocilia "treadmills" and the whole stereocilium core is replaced within 48 hours (Schneider et al. 2002; Rzadzinska et al. 2004), recent studies demonstrated that the auditory hair cell stereocilia are in fact very stable in normal physiological conditions with the exception of a limited area at the very tips of stereocilia (Zhang et al. 2012; Drummond et al. 2015; Narayanan et al. 2015). In the second and third row stereocilia that harbor mechanotransduction channels (Beurg et al. 2009), the remarkable stability of the actin core is maintained by the Ca^{2+} influx through these channels (Velez-Ortega et al. 2017). The stability of the tallest row stereocilia, which do not possess mechanotransduction channels (Beurg et al. 2009), may be related to the cell signaling mechanisms that underlie the stability of microvilli when they become interconnected by fine extracellular links (Gorelik et al. 2003). It is well known that the postnatal maturation of both IHC and OHC stereocilia includes formation of the numerous transient inter-stereocilia links and their transitioning to well-defined mature links (Goodyear et al. 2005; Petit and Richardson 2009). The cochlear epithelium seems to have a global program that reduces during development any "unneeded" microvilli-like structures, except for the ones that are "protected" either by the Ca^{2+} influx or by the extracellular links. This retraction is not restricted to the hair cells but extends also to the microvilli in the rim borders of neighboring supporting cells—see SEM images of IHC and OHC bundles starting from P10 and beyond in Figs. 2 and 3, respectively. According to our data, this retraction is largely present in $Myo15^{sh2/sh2}$ and $Myo15^{\Delta N/\Delta N}$ cochlear epithelia and is therefore independent of myosin-XVa.

Short Isoform of Myosin-XVa Is Essential for Stereocilia Thickness Gradation Within the Auditory Hair Cell Bundles

It has been established that myosin-XVa is essential for the programmed elongation of stereocilia in development by delivering its cargo whirlin and other components of the stereocilia elongation complex to the tips of the stereocilia (Belyantseva et al. 2005). However, the role of myosin-XVa in the control of other features of hair cell architecture, such as the diameter of stereocilia, has not been yet investigated. Our study not only demonstrates the effects of myosin-XVa dysfunction on the thickness of stereocilia in hair cells but also provides quantitative evidence of diameter regulation within a wild-type hair bundle during postnatal development. Out of two published myosin-XVa isoforms, the short isoform is expressed early in development (as early as E18.5 in the basal turn of the cochlea (Belyantseva et al. 2003)) and is necessary and sufficient for the hair bundle growth (Belyantseva et al. 2005). The long isoform is not detectable at the stereocilia tips at P1, becomes prominent there only after P7, and is not essential for hair bundle formation (Fang et al. 2015). Therefore, it is not surprising that the current study found no disruption of stereocilia diameter gradation in $Myo15^{\Delta N/\Delta N}$ hair cells, implying that it is the short isoform of myosin-XVa that is essential for the control of stereocilia diameters.

Building the actin core of a stereocilium requires polymerization of thousands of actin monomers into parallel actin filaments (Tilney et al. 1983; Krey et al. 2016). To maintain this structure, thousands of actin cross-linker proteins connect these filaments to keep the stereocilia stable (Tilney et al. 1983; Krey et al. 2016). In the mammalian auditory hair cells, those proteins are known to be different isoforms of espin, plastin, and fascin (Krey et al. 2016). During development, stereocilia thickness is determined by three key factors (i) the number of actin filaments inside the stereocilium, (ii) the number of actin-associated cross-linker molecules, and (iii) inter-filament distances that are allowed by these cross-linker molecules. In fact, mice that lack plastin alone or together with fascin are deaf and their stereocilia are thinner due to a decrease in the number of actin filaments in the stereocilia cores and the modifications in the packing of these filaments (Krey et al. 2016).

Immunolabeling experiments have shown that cross-linker proteins, espin, plastin, and fascin, are localized only to the shaft of the stereocilia (Krey et al. 2016). These proteins are replaced with the unusual actin bundlers, TRIOBP-4 and TRIOBP-5, at the base of the stereocilia, which allows for flexibility during life-long sound-induced bundle deflections (Kitajiri et al. 2010). Interestingly, none of these proteins localizes to the tips of the stereocilia. Myosin-XVa is the first molecule essential for the control of stereocilia diameters that localizes at the stereocilia tips. It is yet unknown how exactly myosin-XVa regulates the width of a stereocilium. According to our data, myosin-XVa controls the developmental inhibition of the growth of third row stereocilia (Figs. 4d and 5d). Therefore, it cannot simply bring some sort of "thickening" molecules to the stereocilia tips. More likely, myosin-XVa interacts with some yet unknown molecules that are expressed more prominently at the tips of the third row stereocilia to control the number of actin filaments. An interesting protein that interacts with the components of the myosin-XVa-based macromolecular complex (specifically, with whirlin) is "calcium and integrin-binding protein 2," CIB2. CIB2 has been shown to be essential for hair cell mechanotransduction and calcium signaling (Riazuddin et al. 2012). Immunolabeling localized CIB2 to the tips of the third row stereocilia, while SEM imaging revealed growth abnormalities such as increased height of second row stereocilia, occasional degeneration, and increased diameters of the third row stereocilia in IHCs of CIB2 mutants (Giese et al. 2017). Note that we observed a similar thickening of third row stereocilia in *Myo15*$^{sh2/sh2}$ IHCs (Fig. 4e) and OHCs (Fig. 5e).

Myosin-XVa Deficiency May Reveal a Primitive, "Innate" Gradation of Stereocilia Diameters Within a Bundle

It is worth mentioning that myosin-XVa deficiency does not completely eliminate the gradation of stereocilia diameters between stereocilia rows in the hair bundles of *Myo15*$^{sh2/sh2}$ mice. Instead, the diameters become "equally spaced" from the first to the third row in both IHCs and OHCs at the late developmental stages (Figs. 4e and 5e). Considering fourth and fifth rows in *Myo15*$^{sh2/sh2}$ IHCs, this subtle gradient of diameters becomes even more prominent (Fig. 6b). Similar residual height differences between stereocilia of different rows are also seen in *Myo15*$^{sh2/sh2}$ OHCs (Fig. 6f). Of course, all these differences may be caused by degeneration of stereocilia in the mutant *Myo15*$^{sh2/sh2}$ hair cells that progress radially toward the first row. However, a more interesting hypothesis postulates that this gradual morphology of the heights and diameters of different row stereocilia in *Myo15*$^{sh2/sh2}$ hair cells may reflect a gradient of a hypothetical morphogen that determines the fate of a stereocilium in early development. Then, the myosin-XVa-based complex "overrides" these subtle gradients by shaping the hair bundle to the particular needs of sound transduction.

Myosin-XVa-Based Complex Is Likely to Be Involved in the Effects of Mechanotransducer Current on the Hair Bundle Morphology

Inhibition of the resting current through mechanotransduction channels disrupts the stability of stereocilia actin and results in retraction of the transducing second and third row stereocilia in mammalian auditory hair cells (Velez-Ortega et al. 2017). Similar retraction of transducing stereocilia occurs in mutant mice that lack proteins essential for mechanotransduction (Alagramam et al. 2011; Caberlotto et al. 2011). Recently, it has been demonstrated that genetic or pharmacological ablation of mechanotransducer current causes also the loss of diameter gradation between stereocilia rows in IHCs (Krey et al. 2019). This transduction-dependent loss of stereocilia diameter gradation is accompanied by re-distribution of various molecular components of myosin-XVa-based complex between different stereocilia rows within a hair bundle (Krey et al. 2019). The unsolved question is whether these phenomena are unrelated and occur in parallel, or myosin-XVa-based complex indeed controls the gradation of stereocilia diameters within a hair bundle. In this study, we observed the loss of stereocilia diameter gradation in IHCs and OHCs of young postnatal auditory hair cells of homozygous *Myo15*$^{sh2/sh2}$ mice, which lack both isoforms of myosin-XVa in their stereocilia (Belyantseva et al. 2003; Fang et al. 2015). However, these *Myo15*$^{sh2/sh2}$ hair cells have prominent inter-stereocilia links, apparently normal resting current through the mechanotransducer channels in both IHCs and OHCs, and nearly normal transduction responses with the exception of the loss of fast adaptation in IHCs (Stepanyan et al. 2006; Stepanyan and Frolenkov 2009). Therefore, the abnormalities of stereocilia diameters in *Myo15*$^{sh2/sh2}$ mice cannot result from the loss of mechanotransduction and we have to conclude that myosin-XVa-based complex is indeed involved in the mechanotransduction-dependent control of stereocilia diameter gradation within a hair cell bundle.

ACKNOWLEDGMENTS

The study was supported by NIH (R01DC014658 and S10OD025130 to G.I.F. and T32GM118292 support to S.H.). This work was performed in part at the Electron Microscopy Center, which belongs to the National Science Foundation NNCI Kentucky Multiscale Manufacturing and Nano Integration Node, supported by ECCS-1542174.

REFERENCES

ALAGRAMAM KN, GOODYEAR RJ, GENG R, FURNESS DN, VAN AKEN AF, MARCOTTI W, KROS CJ, RICHARDSON GP (2011) Mutations in protocadherin 15 and cadherin 23 affect tip links and mechanotransduction in mammalian sensory hair cells. PLoS One 6:e19183

BARR-GILLESPIE PG (2015) Assembly of hair bundles, an amazing problem for cell biology. Mol Biol Cell 26:2727–2732

BELYANTSEVA IA, BOGER ET, FRIEDMAN TB (2003) Myosin XVa localizes to the tips of inner ear sensory cell stereocilia and is essential for staircase formation of the hair bundle. Proc Natl Acad Sci U S A 100:13958–13963

BELYANTSEVA IA, BOGER ET, NAZ S, FROLENKOV GI, SELLERS JR, AHMED ZM, GRIFFITH AJ, FRIEDMAN TB (2005) Myosin-XVa is required for tip localization of whirlin and differential elongation of hair-cell stereocilia. Nat Cell Biol 7:148–156

BEURG M, FETTIPLACE R, NAM JH, RICCI AJ (2009) Localization of inner hair cell mechanotransducer channels using high-speed calcium imaging. Nat Neurosci 12:553–558

CABERLOTTO E, MICHEL V, FOUCHER I, BAHLOUL A, GOODYEAR RJ, PEPERMANS E, MICHALSKI N, PERFETTINI I, ALEGRIA-PREVOT O, CHARDENOUX S, DO CRUZEIRO M, HARDELIN JP, RICHARDSON GP, AVAN P, WEIL D, PETIT C (2011) Usher type 1G protein sans is a critical component of the tip-link complex, a structure controlling actin polymerization in stereocilia. Proc Natl Acad Sci U S A 108:5825–5830

DELPRAT B, MICHEL V, GOODYEAR R, YAMASAKI Y, MICHALSKI N, EL-AMRAOUI A, PERFETTINI I, LEGRAIN P, RICHARDSON G, HARDELIN JP, PETIT C (2005) Myosin XVa and whirlin, two deafness gene products required for hair bundle growth, are located at the stereocilia tips and interact directly. Hum Mol Genet 14:401–410

DRUMMOND MC, BARZIK M, BIRD JE, ZHANG DS, LECHENE CP, COREY DP, CUNNINGHAM LL, FRIEDMAN TB (2015) Live-cell imaging of actin dynamics reveals mechanisms of stereocilia length regulation in the inner ear. Nat Commun 6:6873

EBRAHIM S, AVENARIUS MR, GRATI M, KREY JF, WINDSOR AM, SOUSA AD, BALLESTEROS A, CUI R, MILLIS BA, SALLES FT, BAIRD MA, DAVIDSON MW, JONES SM, CHOI D, DONG L, RAVAL MH, YENGO CM, BARR-GILLESPIE PG, KACHAR B (2016) Stereocilia-staircase spacing is influenced by myosin III motors and their cargos espin-1 and espin-like. Nat Commun 7:10833

FANG Q, INDZHYKULIAN AA, MUSTAPHA M, RIORDAN GP, DOLAN DF, FRIEDMAN TB, BELYANTSEVA IA, FROLENKOV GI, CAMPER SA, BIRD JE (2015) The 133-kDa N-terminal domain enables myosin 15 to maintain mechanotransducing stereocilia and is essential for hearing. Elife 4. doi: https://doi.org/10.7554/eLife.08627

FURNESS DN, JOHNSON SL, MANOR U, RUTTIGER L, TOCCHETTI A, OFFENHAUSER N, OLT J, GOODYEAR RJ, VIJAYAKUMAR S, DAI Y, HACKNEY CM, FRANZ C, DI FIORE PP, MASETTO S, JONES SM, KNIPPER M, HOLLEY MC, RICHARDSON GP, KACHAR B, MARCOTTI W (2013) Progressive hearing loss and gradual deterioration of sensory hair bundles in the ears of mice lacking the actin-binding protein Eps8L2. Proc Natl Acad Sci U S A 110:13898–13903

GIESE APJ, TANG YQ, SINHA GP, BOWL MR, GOLDRING AC, PARKER A, FREEMAN MJ, BROWN SDM, RIAZUDDIN S, FETTIPLACE R, SCHAFER WR, FROLENKOV GI, AHMED ZM (2017) CIB2 interacts with TMC1 and TMC2 and is essential for mechanotransduction in auditory hair cells. Nat Commun 8:43

GOODYEAR RJ, MARCOTTI W, KROS CJ, RICHARDSON GP (2005) Development and properties of stereociliary link types in hair cells of the mouse cochlea. J Comp Neurol 485:75–85

GORELIK J, SHEVCHUK AI, FROLENKOV GI, DIAKONOV IA, LAB MJ, KROS CJ, RICHARDSON GP, VODYANOY I, EDWARDS CR, KLENERMAN D, KORCHEV YE (2003) Dynamic assembly of surface structures in living cells. Proc Natl Acad Sci U S A 100:5819–5822

KALTENBACH JA, FALZARANO PR, SIMPSON TH (1994) Postnatal development of the hamster cochlea. II Growth and differentiation of stereocilia bundles. J Comp Neurol 350:187–198

KAROLYI IJ, PROBST FJ, BEYER L, ODEH H, DOOTZ G, CHA KB, MARTIN DM, AVRAHAM KB, KOHRMAN D, DOLAN DF, RAPHAEL Y, CAMPER SA (2003) Myo15 function is distinct from Myo6, Myo7a and pirouette genes in development of cochlear stereocilia. Hum Mol Genet 12:2797–2805

KITAJIRI S, SAKAMOTO T, BELYANTSEVA IA, GOODYEAR RJ, STEPANYAN R, FUJIWARA I, BIRD JE, RIAZUDDIN S, RIAZUDDIN S, AHMED ZM, HINSHAW JE, SELLERS J, BARTLES JR, HAMMER JA 3RD, RICHARDSON GP, GRIFFITH AJ, FROLENKOV GI, FRIEDMAN TB (2010) Actin-bundling protein TRIOBP forms resilient rootlets of hair cell stereocilia essential for hearing. Cell 141:786–798

KREY JF, CHATTERJEE P, DUMONT RA, O'SULLIVAN M, CHOI D, BIRD JE, BARR-GILLESPIE PG (2019) Mechanotransduction-dependent control of stereocilia dimensions and row identity in inner hair cells. Curr Biol. https://doi.org/10.1016/j.cub.2019.11.076

KREY JF, KRYSTOFIAK ES, DUMONT RA, VIJAYAKUMAR S, CHOI D, RIVERO F, KACHAR B, JONES SM, BARR-GILLESPIE PG (2016) Plastin 1 widens stereocilia by transforming actin filament packing from hexagonal to liquid. J Cell Biol 215:467–482

LELLI A, MICHEL V, BOUTET DE MONVEL J, CORTESE M, BOSCH-GRAU M, AGHAIE A, PERFETTINI I, DUPONT T, AVAN P, EL-AMRAOUI A, PETIT C (2016) Class III myosins shape the auditory hair bundles by limiting microvilli and stereocilia growth. J Cell Biol 212:231–244

MANOR U, DISANZA A, GRATI M, ANDRADE L, LIN H, DI FIORE PP, SCITA G, KACHAR B (2011) Regulation of stereocilia length by myosin XVa and whirlin depends on the actin-regulatory protein Eps8. Curr Biol 21:167–172

MERRITT RC, MANOR U, SALLES FT, GRATI M, DOSE AC, UNRATH WC, QUINTERO OA, YENGO CM, KACHAR B (2012) Myosin IIIB uses an actin-binding motif in its espin-1 cargo to reach the tips of actin protrusions. Curr Biol 22:320–325

MOGENSEN MM, RZADZINSKA A, STEEL KP (2007) The deaf mouse mutant whirler suggests a role for whirlin in actin filament dynamics and stereocilia development. Cell Motil Cytoskeleton 64:496–508

NARAYANAN P, CHATTERTON P, IKEDA A, IKEDA S, COREY DP, ERVASTI JM, PERRIN BJ (2015) Length regulation of mechanosensitive stereocilia depends on very slow actin dynamics and filament-severing proteins. Nat Commun 6:6855

PENG AW, BELYANTSEVA IA, HSU PD, FRIEDMAN TB, HELLER S (2009) Twinfilin 2 regulates actin filament lengths in cochlear stereocilia. J Neurosci 29:15083–15088

PETIT C, RICHARDSON GP (2009) Linking genes underlying deafness to hair-bundle development and function. Nat Neurosci 12:703–710

PROBST FJ, FRIDELL RA, RAPHAEL Y, SAUNDERS TL, WANG A, LIANG Y, MORELL RJ, TOUCHMAN JW, LYONS RH, NOBEN-TRAUTH K, FRIEDMAN TB, CAMPER SA (1998) Correction of deafness in shaker-2 mice

by an unconventional myosin in a BAC transgene. Science 280:1444–1447

Riazuddin S, Belyantseva IA, Giese AP, Lee K, Indzhykulian AA, Nandamuri SP, Yousaf R, Sinha GP, Lee S, Terrell D, Hegde RS, Ali RA, Anwar S, Andrade-Elizondo PB, Sirmaci A, Parise LV, Basit S, Wali A, Ayub M, Ansar M, Ahmad W, Khan SN, Akram J, Tekin M, Riazuddin S, Cook T, Buschbeck EK, Frolenkov GI, Leal SM, Friedman TB, Ahmed ZM (2012) Alterations of the CIB2 calcium- and integrin-binding protein cause usher syndrome type 1J and nonsyndromic deafness DFNB48. Nat Genet 44:1265–1271

Rzadzinska AK, Schneider ME, Davies C, Riordan GP, Kachar B (2004) An actin molecular treadmill and myosins maintain stereocilia functional architecture and self-renewal. J Cell Biol 164:887–897

Salles FT, Merritt RC Jr, Manor U, Dougherty GW, Sousa AD, Moore JE, Yengo CM, Dose AC, Kachar B (2009) Myosin IIIa boosts elongation of stereocilia by transporting espin 1 to the plus ends of actin filaments. Nat Cell Biol 11:443–450

Schneider ME, Belyantseva IA, Azevedo RB, Kachar B (2002) Rapid renewal of auditory hair bundles. Nature 418:837–838

Schneider ME, Dose AC, Salles FT, Chang W, Erickson FL, Burnside B, Kachar B (2006) A new compartment at stereocilia tips defined by spatial and temporal patterns of myosin IIIa expression. J Neurosci 26:10243–10252

Sekerkova G, Richter CP, Bartles JR (2011) Roles of the espin actin-bundling proteins in the morphogenesis and stabilization of hair cell stereocilia revealed in CBA/CaJ congenic jerker mice. PLoS Genet 7:e1002032

Stepanyan R, Frolenkov GI (2009) Fast adaptation and Ca2+ sensitivity of the mechanotransducer require myosin-XVa in inner but not outer cochlear hair cells. J Neurosci 29:4023–4034

Stepanyan R, Belyantseva IA, Griffith AJ, Friedman TB, Frolenkov GI (2006) Auditory mechanotransduction in the absence of functional myosin-XVa. J Physiol 576:801–808

Tadenev ALD, Akturk A, Devanney N, Mathur PD, Clark AM, Yang J, Tarchini B (2019) GPSM2-GNAI specifies the tallest stereocilia and defines hair bundle row identity. Curr Biol 29(921–934):e924. https://doi.org/10.1016/j.cub.2019.01.051

Tilney LG, Tilney MS (1986) Functional organization of the cytoskeleton. Hear Res 22:55–77

Tilney LG, Derosier DJ, Mulroy MJ (1980) The organization of actin filaments in the stereocilia of cochlear hair cells. J Cell Biol 86:244–259

Tilney LG, Tilney MS, DeRosier DJ (1992) Actin filaments, stereocilia, and hair cells: how cells count and measure. Annu Rev Cell Biol 8:257–274

Tilney LG, Egelman EH, DeRosier DJ, Saunder JC (1983) Actin filaments, stereocilia, and hair cells of the bird cochlea. II. Packing of actin filaments in the stereocilia and in the cuticular plate and what happens to the organization when the stereocilia are bent. J Cell Biol 96:822–834

Velez-Ortega AC, Freeman MJ, Indzhykulian AA, Grossheim JM, Frolenkov GI (2017) Mechanotransduction current is essential for stability of the transducing stereocilia in mammalian auditory hair cells. Elife 6:e24661. https://doi.org/10.7554/eLife.24661

Wang A, Liang Y, Fridell RA, Probst FJ, Wilcox ER, Touchman JW, Morton CC, Morell RJ, Noben-Trauth K, Camper SA, Friedman TB (1998) Association of unconventional myosin MYO15 mutations with human nonsyndromic deafness DFNB3. Science 280:1447–1451

Zampini V, Ruttiger L, Johnson SL, Franz C, Furness DN, Waldhaus J, Xiong H, Hackney CM, Holley MC, Offenhauser N, Di Fiore PP, Knipper M, Masetto S, Marcotti W (2011) Eps8 regulates hair bundle length and functional maturation of mammalian auditory hair cells. PLoS Biol 9:e1001048

Zhang DS, Piazza V, Perrin BJ, Rzadzinska AK, Poczatek JC, Wang M, Prosser HM, Ervasti JM, Corey DP, Lechene CP (2012) Multi-isotope imaging mass spectrometry reveals slow protein turnover in hair-cell stereocilia. Nature 481:520–524